Received: 14 March 2018 | Revised: 13 September 2018 | Accepted: 5 October 2018

DOI: 10.1002/er.4278

RESEARCH ARTICLE

WILEY INTERNATIONAL JOURNAL OF ENERGY RESEARCH

Analytical approach to ground heat losses for high temperature thermal storage systems

Christian Suárez | Javier Pino | Felipe Rosa | Jose Guerra

Escuela Superior de Ingenieros, DIE—Grupo de Termotecnia, University of Seville, Avda. Descubrimientos s/n, 41092 Seville, Spain

Correspondence
Christian Suárez, Escuela Superior de Ingenieros, DIE—Grupo de Termotecnia, University of Seville, Avda. Descubrimientos s/n, 41092 Seville, Spain.
Email: chss@us.es

Summary

A new approach to estimate the heat loss from thermal energy storage tank foundations is presented. Results are presented through analytical correlations based on numerical solutions for the steady-state heat conduction problem for thermal energy slab-on-grade tanks with uniform insulation. Model results were verified with other well-established benchmark problems with similar boundary conditions and validated with experimental data with excellent agreement. In addition to the TES foundation heat loss, new correlations for the maximum temperature and for the radial evolution of the temperature underneath the insulation layer are also provided, giving important information related to the tank foundation design. The correlated variables are of primordial importance in the tank foundation design because, due to the typical high operating storage temperatures, an inappropriate tank foundation insulation would lead not only to a not desired loss of energy but also to an inadmissible increase of the temperatures underneath the insulation layer, affecting the structural stability of the tank. The proposed correlations provide a quick method for the estimation of total tank foundation heat losses and soil maximum temperature reached underneath the insulation layer, saving time, and cost on the engineering tank foundation design process. Finally, a comprehensive parametric analysis of the variables of interest is made and a set of cases covering a wide range of tank sizes, insulation levels, depths to water table, and storage temperatures are solved.

KEYWORDS

ground, heat loss, tank, TES

Nomenclature: D, Dimensionless insulation; D', Depth, m; ND, Non-dimensional; N, Number of nodes; Q, Heat flux, W; q, Heat flux density, W m^{-2}; r, Radial direction, m; r^*, Dimensionless radius; R, Tank radius, m; R', Thermal resistance, m^2 K W^{-1}; T, Temperature, °C; t, Thickness, m; z, Axial direction, m; Z, Dimensionless water table depth **Greek Letters:** λ, Thermal conductivity, W m^{-1} K^{-1}; θ, Dimensionless temperature **Subscripts:** avg, Average; dom, Domain; eq, Equivalent; ext, Exterior; ins, Insulation; max, Maximum; stg, Storage; wt, Water table; *x_ext*, X direction below exterior air; *x_tank*, X direction below the tank; *x_total*, X direction total

1 | INTRODUCTION

Concentrated solar power in combination with thermal energy storage (TES) has the distinctive advantage in comparison with other sources of renewable energy that its generated energy can be collected and shifted over time, solving the mismatch between solar energy supply and electricity demand. The most commercially accepted thermal storage design, which have demonstrated reliable operation at commercial-scale within their capable temperatures, is an indirect two-tank molten salt storage system. In this storage design, molten salt interacts with the solar field heat transfer fluid through a heat exchanger and is collected separately at different temperature levels in the denominated "cold" and "hot" tanks. TES systems' temperature levels in utility-scale solar power plants (SPPs) vary depending on the application, reaching typically temperatures of 292°C to 386°C for parabolic trough plants and 292°C to 565°C for central receiver plants with molten salts. Molten salt-based TES systems despite having low overall efficiencies have relatively low capital costs as well, which makes them a good candidate for TES systems.[1]

Thermal energy storage is a key component of any successful thermal system, and a good TES should allow minimum thermal energy losses, leading to energy savings, while permitting the highest possible extraction efficiency of the stored thermal energy.[2] An adequate tank insulation design is primordial to minimize thermal losses from the tank to the environment through the tank's walls, roof, and foundation. These thermal losses cause the decrease of the storage media temperature and the increase of the tank surroundings temperature, and so a reduction of the TES efficiency. Even though thermal losses through the tank walls and roof represent a more important percentage of the total heat losses when the tank is filled to its maximum charging level, it is also necessary to control the foundation heat losses. Otherwise, it would lead to a not desired loss of energy, with a reduction of TES efficiency. In addition, foundation thermal losses have other adverse thermal effects in the molten salt and the soil underneath the tank. An appropriate insulation of the foundation is necessary because it minimizes the risk of local crystallization of the molten salts at the bottom of the tank. This risk is especially important during long standby periods when the salt mixture has a relatively high crystallization point and when the tank is filled to its maximum charging level, because the minimum local temperatures in the molten salt media are reached at the proximities of the bottom of the tank.[3] This local crystallization risk must be avoided because it would cause the collapse of the entire plant and also because molten salt cost represents the greatest TES cost item, estimated to be about 50% of the total cost.[4] Furthermore, tank material layers and soil underneath the tank must be preserved from reaching temperatures over a maximum admissible value from which the structural properties would be deteriorated, affecting the structural stability of the tank and increasing the risk of total or differential settlements into the ground.

Typical foundation designs in state-of-the-art TES tanks include two main approaches: (1) the combined design of an adequate insulation with a ventilated system of cooling pipes embedded within the foundation; (2) the design of an adequate foundation insulation that provides itself enough thermal protection to the concrete and soil layers underneath the insulation layer. Due to the coupled nature of the problem, heat transfer through the ground has long been recognized as being a substantially more complex problem compared with that through components above ground. While a considerable number of research efforts on ground-coupled heat losses applied to buildings can be found in the open literature with detailed foundation heat losses models,[5-8] including some design guides, such as ASHRAE (1997)[9] or CIBSE (1986),[10] less information in quantity and in level of detail can be found in the field of TES tanks applications. In some works, simplifications in the models for TES applications are excessive, assuming that no heat transfer occurs from the top or the bottom of each tank,[11] or considering only an overall heat transfer coefficient to take into account the total heat losses,[12-14] without distinguishing the contributions of the different parts: wall, top, and bottom. More detailed thermal models to obtain the heat losses in TES tank's plants can be found in references Schulte-Fischedick et al,[15] Zaversky et al,[16] and Rodríguez et al.[17] In these investigations, a tank based on the geometry and operating conditions of the Andasol-1 commercial trough power plant is analyzed, and the heat losses are evaluated. However, although the tank geometry and the operating conditions used were similar, the reported results in terms of the bottom heat losses were quite different between them, with differences above 100%. More recently, Bonilla et al[18] developed a thermal tank model and validated it experimentally in charging and discharging processes and also at rest state to validate thermal losses dynamics. However, in this work, it was only reported the evolution of molten salts and air temperatures inside the tank, being not possible to deduce the tank foundation heat losses separately from the total tank heat losses. Also recently, Prieto et al[19] built a solar power pilot plant with a two-tank solar storage system with molten salts and carried out the experimental evaluation of the temperature distribution inside the tanks and their heat losses. Heat losses

through the walls and top of the tank were measured, and the reported results of 79 and 73 W/m^2, respectively, were successfully verified with a 1-D steady state model. However, in that work, it was specified that in the case of the measured bottom heat losses of 61 W/m^2, the complexity of the model and the lack of literature made impossible the comparison of the experimental results. In a previous work of the present authors,[20] a multilayer analytical model for the estimation of the tank's bottom heat losses in steady state is developed for the case of ventilated foundations, with cooling pipes embedded within the foundation. In that work, the foundation ventilation system is assumed to be designed to establish a constant uniform temperature in the concrete layer below the maximum admissible temperature. A fraction of the total bottom losses is extracted to the environment and the rest is conducted through the soil. The results were discussed in detail through a comprehensive parametric analysis and summarized graphically, providing a quick method for the estimation of the ventilation heat losses and the heat loss to the soil separately. However, results of that previous work cannot be applied to the case of foundations without a ventilation system because in this configuration the temperature underneath the tank is unknown a priori and variable in the radial direction, being the conduction problem different and more complex to solve.

The high differences found in the literature review in the estimation of the bottom heat losses[15-17] and the lack of specific studies applied to TES tank foundation heat losses suggest the necessity of a more accurate calculation method. To address this issue, in the present work, the classical problem of ground-coupled conduction is revised for the practical application of slab on grade TES tanks, providing a quick and accurate method to calculate the tank foundation heat losses. Furthermore, new analytical correlations for the maximum temperature and also for the radial evolution of temperature underneath the insulation layer are also investigated as function of the input parameters. These correlations provide a valuable contribution to TES tank foundation design stage, in which it must be verified that the soil underneath the tank is preserved from reaching excessive temperatures. According to the authors' best knowledge, no publications can be found in the literature providing such an analytical method addressing this particular issue.

2 | METHODOLOGY

The problem formulation and the solution procedure are presented in this section. Furthermore, the mathematical model and the main characteristics of the numerical approach are also described and justified through a verification and validation process with other well-established benchmark problems and experimental data.

2.1 | Description of the problem

The sketch of a cylindrical slab-on-grade storage tank of radius R with uniform insulation, thickness t_{ins}, and thermal conductivity λ_{ins} is shown in Figure 1. The ground underneath the tank is considered to be homogeneous having a constant thermal conductivity λ. Both cases unsaturated and saturated soils are studied in the research. For the case of saturated soils, a constant temperature T_{wt} throughout the year is fixed at the water table depth D'_{wt}. The tank's bottom heat losses occur through the slab foundation due to the temperature gradient that exist between the interior storage tank temperature (T_{stg}) and the environment, represented by the annual mean outdoor temperature (T_{ext}) and annual mean water table temperature (T_{wt}).

State-of-the-art TES tank foundations typically consist of a thin steel slip plate layer followed by a thin layer of dry sand, a foam glass insulation layer, and a concrete thermal foundation.[15-17,21-23] With the objective to simplify the model, only an equivalent thermal layer, with the total thermal resistance of the foundation layers considered in series, is assumed in the model. This assumption is an acceptable and conservative approach because in most practical situations, the thermal resistance of the slip plate, the sand, and the concrete layer are negligible in comparison to the foam glass insulation one. Furthermore, the footings of the foundation, usually made of concrete with a thermal conductivity similar to that of the ground in most cases, are considered as integral parts for the soil medium. The analysis presented in this paper considers the annual average thermal performance of the foundation and, thus, is limited to steady-state conditions.

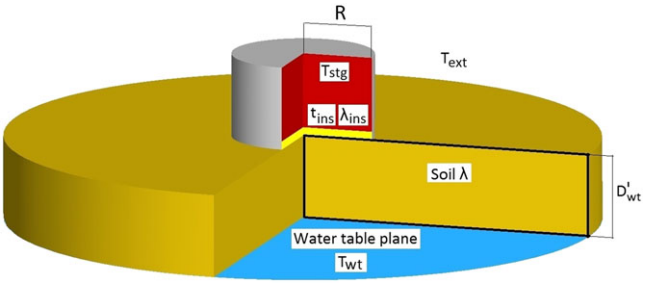

FIGURE 1 Sketch of a cylindrical slab-on-grade storage tank [Colour figure can be viewed at wileyonlinelibrary.com]

2.2 | Solution procedure

A scheme of the solution procedure performed in this paper is summarized in Figure 2. A numerical model is developed to analyze the steady-state conduction heat transfer problem that takes place in TES slab on grade tank's foundation. Simulation results are firstly validated and verified with other published results in the open literature. Special attention is paid to the next variables: maximum temperature achieved underneath the insulation layer (T_{max}), radial evolution of the bottom temperature ($T_{bottom}(r)$), and total bottom heat losses Q_{bottom}. A comprehensive set of numerical simulations is made covering a wide range of tank sizes (tank radii R), depths to water table D'_{wt}, insulation thermal resistances, and storage temperatures. Simulation results of T_{max} and $T_{bottom}(r)$ are then correlated with appropriate mathematical functions which depend on the previously described input parameters. An expression for total bottom heat losses Q_{bottom} is inferred from the correlation of $T_{bottom}(r)$ and verified with the simulation results.

2.3 | Numerical method

The developed numerical model is described in this section, with special emphasis in the description of the model and its boundary conditions (BCs) and the verification and validation process. A computational size and mesh independence study is also included in the analysis.

2.3.1 | Model description, governing equations, and BCs

Taking advantage of the axisymmetric geometry of the problem, the 3D problem can be simplified to a 2D axisymmetric one of dimensions r_{dom} and z_{dom} representing the soil underneath the tank. Commercial software ANSYS Fluent 14.0 (ANSYS, Inc., Southpointe, Canonsburg, PA, USA) is used to solve numerically the 2D steady-state heat conduction equation in cylindrical coordinates[24]:

$$\frac{1}{r}\frac{\partial}{\partial r}\left(r\frac{\partial T}{\partial r}\right)+\frac{\partial^2 T}{\partial z^2}=0;\ 0\le r\le r_{dom};0\le z\le z_{dom}. \quad (1)$$

With the following BCs:

$$\text{Axisymmetric axis BC,}\quad \frac{\partial T}{\partial r}(0,z)=0;\ 0\le z\le z_{dom} \quad (2)$$

$$\text{Adiabatic far field BC,}\quad \frac{\partial T}{\partial r}(r_{dom},\ z)=0;\ 0\le z\le z_{dom} \quad (3)$$

$$\text{Isothermal BC, unsaturated soils,}\quad T(r,z_{dom})=T_{ext} \quad (4)$$

$$\text{Isothermal BC, saturated soils,}\quad T(r,z_{dom})=T_{wt} \quad (5)$$

$$\text{Isothermal BC, thin layer material,}\quad T(r,0)=T_{stg}-\frac{t_{ins}}{\lambda_{ins}};\ 0\le r\le R \quad (6)$$

$$\text{Isothermal BC, external temperature,}\quad T(r,0)=T_{ext};\ R\le r\le r_{dom} \quad (7)$$

Defined BCs are imposed directly in the limits of the 2D computational domain ($r_{dom} \times z_{dom}$), as depicted in Figure 3.

Axisymmetric axis and adiabatic wall BCs at the far-field distance are imposed in the vertical limits of the domain (Equations 2 and 3). For the case of unsaturated soils, constant uniform temperature distribution equal to the deep ground soil temperature is imposed at $z = z_{dom}$, as indicated in Equation 4. This uniform temperature distribution in the deep soil layers, in which the temperature

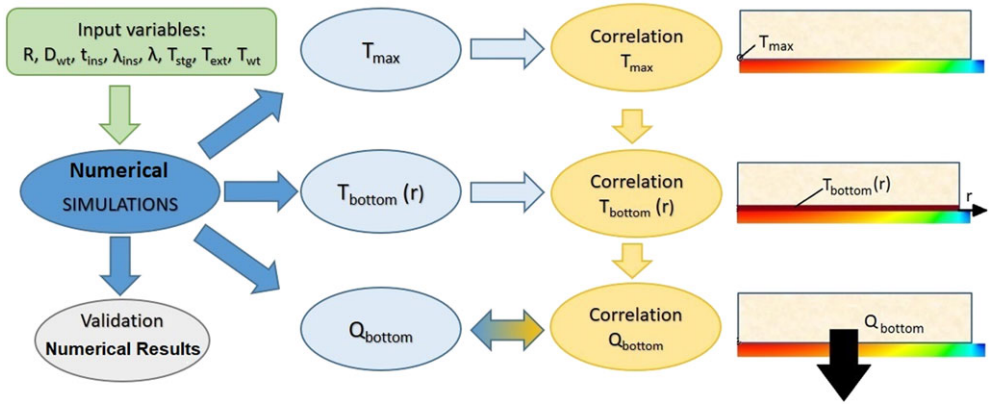

FIGURE 2 Solution procedure [Colour figure can be viewed at wileyonlinelibrary.com]

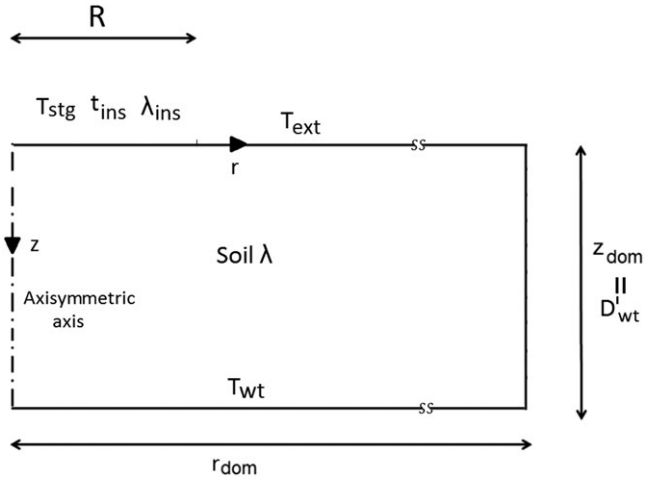

FIGURE 3 Computational domain and boundary conditions

distribution remains unchanged throughout the year, can be taken as a first approach as the annual mean outdoor temperature.[20,25,26] For saturated soils, a constant uniform temperature distribution is fixed in the water table depth as indicated in Equation 5. The water table temperature (T_{wt}) is assumed to be the same as the annual mean outdoor temperature (T_{ext}). The storage tank temperature is modeled using an isothermal BC, in which the effect of the tank bottom insulation is also considered and specified on the outside of the solid domain, defining a thin wall material of insulation thickness t_{ins} and thermal conductivity λ_{ins} as indicated in Equation 6. Exterior temperature is modeled using an isothermal BC (Equation 7).

2.3.2 | Verification and validation of the numerical results

In this section, the performed verification and validation of the numerical results are described. In order to verify the mathematical model and the procedure of the investigated numerical approach, the results of the present work were compared with other similar well-established benchmark problems. To the best of the author's knowledge, no experimental studies have been published measuring the TES tank's foundation heat losses or the soil temperatures underneath the tanks in real-scale SPP. However, it was possible to find in the open literature other investigations related to the heat losses through the foundation for building applications and also a pilot-scale tank experimental evaluation of the bottom heat losses. Results reported in the area of building foundations,[7,8] which have the same circular foundation geometry and similar BCs in comparison to the present research problem, are used as a benchmark to verify the numerical results of the present work in terms of bottom heat losses and soil isotherms. Firstly, the numerical results obtained by Hagentoft[7] for the steady-state heat losses in a circular slab are used as a benchmark to establish the computational domain size and mesh refinement of the proposed numerical model. Secondly, the results in terms of the soil isotherms are compared with the results reported by Chuangchid and Krarti[8] to gain confidence in the numerical model setup. Finally, numerical results are validated with the experimental results of the bottom heat losses obtained by Prieto et al[19] in a pilot-scale TES tank.

2.3.3 | Model computational size and grid independence study

An analysis of the amount of soil to model, defined by the far-field distance r_{dom} and deep ground distance z_{dom}, and the number of nodes and its distribution is developed for two insulated circular slabs of 20-m radius over a sandy unsaturated soil with a thermal conductivity of $\lambda = 2$ W/mK. Temperature difference is fixed at 100°C, and the considered thermal insulations are 40 and 80 cm for cases 1 and 2, respectively, with an insulation thermal conductivity of $\lambda_{ins} = 0.06$ W/mK. Results obtained using the expression proposed by Hagentoft[7] for the heat loss through the slab bottom, Q_{bottom}, are used as reference results. He considered a circular slab of radius R, insulation thickness t_{ins}, and thermal conductivity λ_{ins} supported directly upon a soil of thermal conductivity λ, as shown in Figure 4. The temperature above the slab is T_i, and the temperature at the deep-ground soil is T_{soil}.

He proposed the following expression for the calculation of the bottom heat losses[7]:

$$Q_{bottom} = \lambda \cdot (T_i - T_{soil}) \cdot R \cdot h_{sc}\left({}^{d}/_{R}\right) \tag{8}$$

where d is the soil equivalent insulation thickness defined by

$$d = t_{ins}\left(\frac{\lambda}{\lambda_{ins}}\right) \tag{9}$$

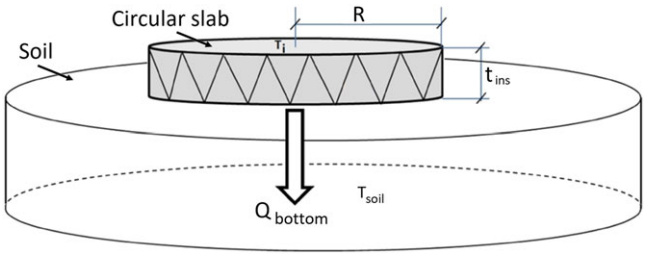

FIGURE 4 Sketch of a circular slab-on-grade foundation [Colour figure can be viewed at wileyonlinelibrary.com]

and h_{sc} (d/R) is the heat loss factor, which depends on the parameter d/R. For slabs with thick insulations ($d/R > 0.6$), the heat loss factor can be approximated with an error below a 3% in comparison with numerical results with the expression:

$$h_{sc}\left({}^{d}/_{R}\right) = \frac{\pi}{{}^{d}/_{R} + {}^{4}/_{3\pi}}. \quad (10)$$

Firstly, an independence study is performed for three different domain sizes (2R × 2R, 5R × 5R, and 9R × 9R), keeping approximately fixed the mesh size with a grading ratio of 1.01 in both radial and depth directions, taking the reference at the point (r,z) = (R,0). Results included in Table 1 indicate that an enlarged domain of r_{dom} = 5R and z_{dom} = 5R or equivalently of 100 m × 100 m was enough to properly model the problem, with a maximum error of 2.2% in comparison with the reference results. The benefits in the accuracy in terms of the results of the use of a longer computational domain of dimensions 9R × 9R of only a 0.2% in comparison with the benchmark data are not justified due to the high increase of the computational time in the simulations.

Secondly, an independence study is performed for three different mesh densities of 10 000, 40 000, and 72 000 nodes, respectively, keeping fixed an enlarged domain of r_{dom} = 5R and z_{dom} = 5R and a grading ratio or 1.01. Results included in Table 2 show very similar results in terms of the bottom heat losses for the three mesh densities, with differences in the accuracy of the results below a 0.1%. The mesh size of 40 000 nodes is chosen, with a maximum error of 2.2% in comparison with the reference results. The coarsest mesh of 10 000 nodes, although also giving good results, was discarded in an effort to improve accuracy of local results in regions near the tank foundation where temperature gradients are expected to be high. The finest mesh of 72 000 nodes was not considered because the obtained benefit in the results accuracy of only 0.1% in comparison with the chosen mesh is not justified due to the significant increase of the computation time.

From this sensitivity analysis, an enlarged domain of r_{dom}/R = 5 and z_{dom}/R = 5 and a mesh size of 40 000 nodes is selected for the computational model. In Figure 5, a sketch of the selected computational domain and mesh density is shown. A numerical model with these characteristics is used hereafter to solve the conductive problem in the soil underneath the TES tanks.

2.3.4 | Total bottom heat losses verification

Further verifications were done to compare the results of the present work in terms of the bottom heat losses with

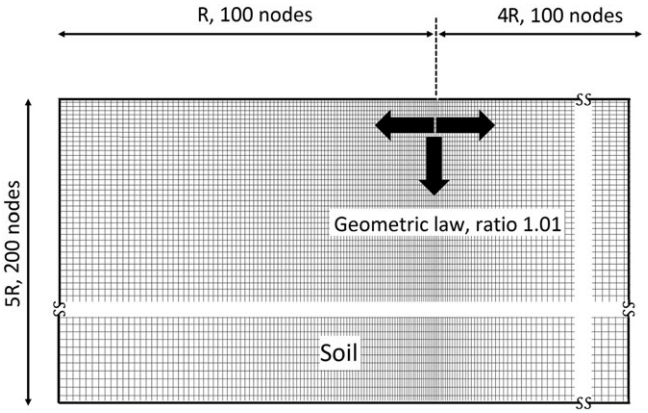

FIGURE 5 Selected computational domain and mesh density

TABLE 1 Soil domain size sensitivity analysis

Case	r_{dom}/R	z_{dom}/R	N_{r_R}	N_{r_ext}	N_{r_total}	N_z	N_{total}	Q1 (W)	Q2 (W)
1	2	2	100	100	200	150	30 000	11 806	7212
2	5	5	100	100	200	200	40 000	11 778	7201
3	9	9	125	250	375	275	103 125	11 756	7193
Hagentoft7	-	-	-	-	-	-	-	11 517	7149

TABLE 2 Soil domain mesh sensitivity analysis

Case	r_{dom}/R	z_{dom}/R	N_{r_R}	N_{r_ext}	N_{r_total}	N_z	N_{total}	Q1 (W)	Q2 (W)
1	5	5	50	50	100	100	10 000	11 773	7198
2	5	5	100	100	200	200	40 000	11 778	7200
3	5	5	150	180	330	400	72 000	11 782	7202
Hagentoft7	-	-	-	-	-	-	-	11 517	7149

the results obtained using the expressions proposed by Hagentoft[7] in Equations 8 to 10. A total of 16 numerical simulations were performed for two slabs of 10 and 20 m of radii and different insulation levels, ranging from 0.4 to 1 m and from 0.2 to 1 m with steps of 0.1 m of insulation thickness, respectively. The rest of the parameters were kept constant ($\lambda = 2$ W/m K, $\lambda_{ins} = 0.06$ W/m K, and T_i-$T_{soil} = 100$°C). Results are shown in Figure 6.

Soil isotherms verification

In addition to the total bottom heat losses verification described in the previous section, further verification is made in terms of the temperature distribution underneath the slab to test the selected numerical model setup. In the verification case, it is considered a water table at a depth of 5 m below the soil surface with a constant temperature of $T_{wt} = 10$°C. Room air temperature above the slab is 20°C, and the annual average ambient air temperature is $T_{ext} = 15$°C. In Figure 7, the numerical results reported by Chuangchid and Krarti[8] for the soil temperature distribution for isotherms ranging from 11°C to 19°C on ground floors without any thermal insulation (cross points) are compared against the results obtained in the present work (solid lines), with excellent agreement between them.

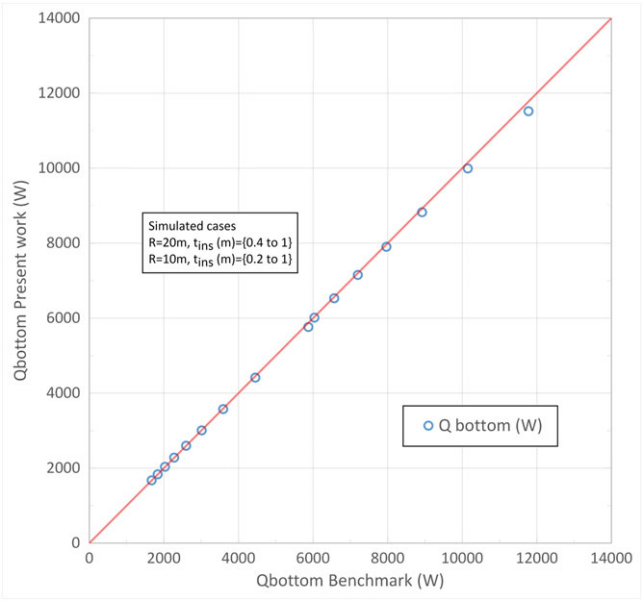

FIGURE 6 Total bottom heat losses verification. Present work vs Hagentoft benchmark results[7] [Colour figure can be viewed at wileyonlinelibrary.com]

Bottom heat losses validation

The bottom heat losses per unit area results obtained in the present work are validated with the experimental results obtained by Prieto et al[19] in a solar power pilot-scale plant in Lérida (Spain). They built a solar power pilot plant with a two-tank solar storage system with molten salts and carried out the experimental evaluation of the temperature distribution inside one of the storage tanks of 1.2 m of internal diameter. They also measured the tank heat losses, reporting a bottom heat loss of 61 W/m^2. In order to evaluate the bottom heat losses, surface temperature sensors (PT-100) were used and placed in the transition of different materials, particularly between the storage tank and the upper foundation material layer (T_{bottom}) and between the lower foundation material layer and the ground (T_{Ground}). The measured values during the steady-state experiment were 369.5°C and 32.6°C, respectively, for T_{bottom} and T_{Ground}. Using Fourier's law of heat conduction,[21] it is straightforward to obtain the experimental equivalent thermal resistance of the bottom foundation (Equation 11).

$$R'_{ins} = \frac{(T_{bottom} - T_{Ground})}{q_{bottom}} = 5.51\ m^2K/W \qquad (11)$$

Numerical simulations were performed with the model setup defined for the same tank radius and thermal resistance parameters ($R = 0.6$ m, $R'_{ins} = 5.51$ m^2 K/W). In the absence of experimental data of the exterior temperature measurements and soil characteristics, T_{ext}

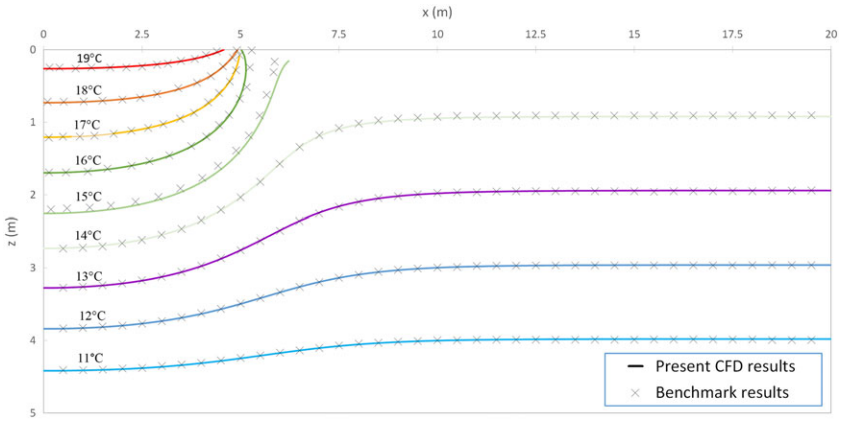

FIGURE 7 Soil isotherms verification. Present work vs Chuangchid and Krarti benchmark results[8] [Colour figure can be viewed at wileyonlinelibrary.com]

is fixed to 15°C (typical value of the average annual temperature in Lérida), and an unsaturated sandy soil (thermal conductivity of 2 W/mK) is assumed for the base case. The obtained simulated result of the bottom heat losses per unit area was 62.81 W/m^2, showing an excellent agreement with the experimental results, with an error of only a 3.0%. In order to estimate and delimit the error caused by the uncertainty in the input parameters of exterior temperature and type of soil, nine additional scenarios were considered, covering the combination of three different exterior temperatures of 10°C, 20°C, and 30°C and three different types of soils: clay, sand, and rock with thermal conductivities of 1.5, 2, and 3.5 W/mK, respectively. Simulation results are presented and compared with the experimental results in Table 3. Results show that numerical simulations can accurately predict the bottom heat losses. The predicted bottom heat losses vary in the range of 59.7 to 64.32 W/m^2 depending on the exterior temperature and type of soil, with deviations below 5.5% in the worst considered scenario (T_{ext} = 10°C and rocky soil) in comparison with the experimental measurement reported by Prieto et al.[19]

2.4 | Dimensionless variables

Using the described numerical model, a comprehensive set of 120 cases of tanks with different radii, levels of insulation, and water table depths were simulated and analyzed in terms of the variables of interests: (1) T_{max}, maximum temperature under the insulation layer; (2) T_{bottom} (r), radial temperature evolution in the tank bottom surface; and (3) Q_{bottom}, total bottom heat losses. T_{max} is reached in the intersection of the tank foundation in contact with the ground with the symmetry axis of storage tank. As the temperature of the soil at any depth is below this value, this variable is a useful indicator for the tank insulation design. The radial evolution of T_{bottom} (r) is also studied in this research. By knowing T_{bottom} (r), total heat losses can be inferred from solving the integral form of Fourier's Law:

$$Q_{bottom} = \int_{r=0}^{r=R} \frac{\left(T_{stg} - T_{bottom}(r)\right)}{t_{ins}/k_{ins}} 2\pi r \, dr = \int_{r=0}^{r=R} \frac{\left(T_{stg} - T_{bottom}(r)\right)}{R'_{ins}} 2\pi r \, dr \quad (12)$$

where T_{stg} is the storage temperature and R'_{ins} is the equivalent insulation thermal resistance, defined as the ratio between the insulation thickness t_{ins} and the insulation thermal conductivity λ_{ins}. Both T_{stg} and R'_{ins} are assumed to be constant.

To reduce the number of input independent variables in the problem, a set of dimensionless variables is defined: (1) dimensionless radius $r^* = r/R$; (2) dimensionless depth $Z = z/R$; and (3) dimensionless equivalent insulation $D_{eq} = d/R$, where the same definition used in Hagentoft[7] is used for the equivalent insulation thickness $d = t_{ins} \cdot \lambda/\lambda_{ins}$.

A dimensionless temperature is defined in Equation 13:

$$\theta = \frac{T - T_{ext}}{T_{stg} - T_{ext}} = \frac{T - T_{ext}}{\Delta T}. \quad (13)$$

With this definition, temperature is scaled, being the lowest possible value $\theta = 0$ for $T = T_{ext}$ and the highest possible value $\theta = 1$ for $T = T_{stg}$. Maximum soil temperatures are reached underneath the tank axis at $z = 0$. Particularizing Equation 13, the corresponding maximum dimensionless temperature (θ_{max}) is defined as

TABLE 3 Bottom heat losses per unit area validation. Present work vs experimental results[19]

Case	Text, °C	Type of soil	λ, W/mK	q, W/m^2	Error, %
Base	15	Sand	2	62.81	3.0
1	10	Clay	1.5	63.22	3.6
2	10	Sand	2	63.69	4.4
3	10	Rock	3.5	64.32	5.4
4	20	Clay	1.5	61.46	0.8
5	20	Sand	2	61.92	1.5
6	20	Rock	3.5	62.53	2.5
7	30	Clay	1.5	59.7	−2.1
8	30	Sand	2	60.15	−1.4
9	30	Rock	3.5	60.74	−0.4
Prieto et al19	-	-	-	61.00	-

$$\theta_{max} = \frac{T_{max} - T_{ext}}{T_{stg} - T_{ext}}. \quad (14)$$

The main dimensionless variables affecting the bottom heat losses are the insulation level, determined by the dimensionless equivalent insulation D_{eq}, and the water table depth, determined by the dimensionless depth Z. Simulation results of θ_{max} and $\theta_{bottom}(r)$ are correlated with proper functions which depend on the previously described dimensionless input parameters D_{eq} and Z. Then, operating with Equations 13 and 14, T_{max} and $T_{bottom}(r)$ are obtained, and an expression for the total bottom heat losses Q_{bottom} is inferred by solving the integral in Equation 12 and verified with the simulation results.

3 | RESULTS AND DISCUSSION

Correlations of the variables of interest based on the simulation results are presented in this section. Furthermore, a parametric analysis is performed using the proposed correlations for the estimation of bottom density heat flux q_{bottom} for TES tanks applications.

3.1 | Simulated cases

A comprehensive set of 120 cases of TES tanks with different radii, levels of insulation, and water table depths were simulated and analyzed. The variation in the input data is summarized in Table 4.

Firstly, numerical results were analyzed in terms of the ND (non-dimensional) variables of interests: θ_{max}, θ_{bottom} (r^*). Thereafter, the dimensional variables T_{max}, $T_{bottom}(r)$, and Q_{bottom} were derived.

3.2 | θ_{max} simulation results and proposed correlation for T_{max}

The ND maximum temperature results obtained with the numerical simulations are analyzed in this section, and a correlation as a function of the ND independent variables D_{eq} and Z is proposed to estimate the simulated results.

In Figure 8, simulation results in dimensionless terms are shown for the evolution of the ND maximum temperature as a function of the ND water table depth Z = D′/R for different values of the ND insulation level D_{eq} = d/R.

Two regions can be distinguished, one for low water table depths, values of $Z = D'_{wt}/R \leq 1$, in which important variations of θ_{max} are observed and its complementary region, values of $Z = D'_{wt}/R > 1$, in which θ_{max} remains approximately constant for each D_{eq} value. From this results, it can be derived that only in the cases in which water table depths are lower than the tank radii, the water table depth has an impact on the maximum temperature reached underneath the tank.

In a preliminary analysis, different mathematical functions were tested against the simulation results shown in Figure 8 for a fixed value of D_{eq}. From this preliminary analysis, a mathematical function of the form presented in Equation 15 is selected to properly fit the simulation results (c_1, c_2, and c_3 are constants for each fixed D_{eq} value).

$$\theta_{max}(Z) = c_1 \cdot [1 - \exp(c_2 Z^{c_3})] \quad (15)$$

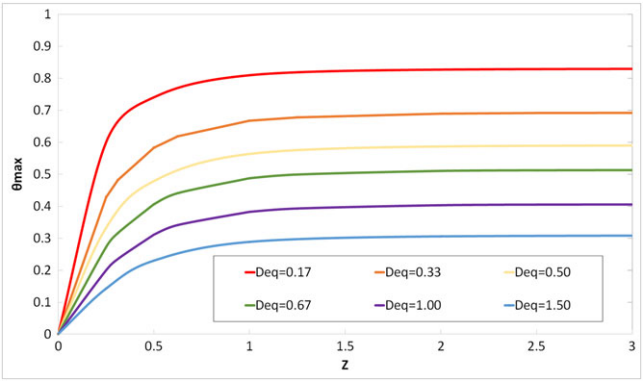

FIGURE 8 ND maximum temperature θ_{max} as a function of ND water depth Z and ND insulation level D_{eq} [Colour figure can be viewed at wileyonlinelibrary.com]

TABLE 4 Input data of simulated cases

Variable. Fixed parameters: T_{ms} = 110°C, T_{ext} = 10°C, λ = 2 W/mK.		
Tank radius R (m)	20	10
Dimensionless radius r*	r*ϵ [0,1]	r*ϵ [0,1]
Water table depth (m)	None, 40, 20, 10, 5 (5 values)	None, 25, 12.5,10, 6.25, 5, 3.125 (7 values)
Dimensionless water table depth Z	Z ϵ [0,5]	Z ϵ [0,5]
Insulation thermal resistance R'_{ins} (m^2/WK)	1.67-16.67 (10 values)	1.67-16.67 (10 values)
Dimensionless equivalent insulation D_{eq}	D_{eq} ϵ{0.17-1.67} (10 values)	D_{eq} ϵ{0.33-3.33} (10 values)
Simulated cases	50	70
Total simulated cases	120	

The proposed correlation for θ_{max}, as a function of the ND parameters D_{eq} and Z, has the mathematical form given by Equation 16:

$$\theta_{max}(D_{eq},Z) = f_1(D_{eq})\cdot\left[1-\exp\left(g_1(D_{eq})Z^{h_1(D_{eq})}\right)\right] \quad (16)$$

where $f_1(D_{eq})$, $g_1(D_{eq})$, and $h_1(D_{eq})$ are functions exclusively of the ND insulation level defined in Equations 17, 18, and 19:

$$f_1(D_{eq}) = \frac{1.05}{1+1.49\cdot D_{eq}} \quad (17)$$

$$g_1(D_{eq}) = -2.35 + \frac{0.6}{D_{eq}^{0.5}} \quad (18)$$

$$h_1(D_{eq}) = \frac{1.13\cdot D_{eq}}{0.075+0.075\cdot D_{eq}} \quad (19)$$

θ_{max} correlation results are compared with the simulation results in Figure 9, where the 45° red solid line indicates a perfect fit between them.

Coefficients used in the proposed correlation have been adjusted in a way that the results are conservative, obtaining values of θ_{max} higher than the simulation results. A good agreement between the correlation and the simulation results was found with an average error of 4.7% and a maximum error of 9.5% in the worst case.

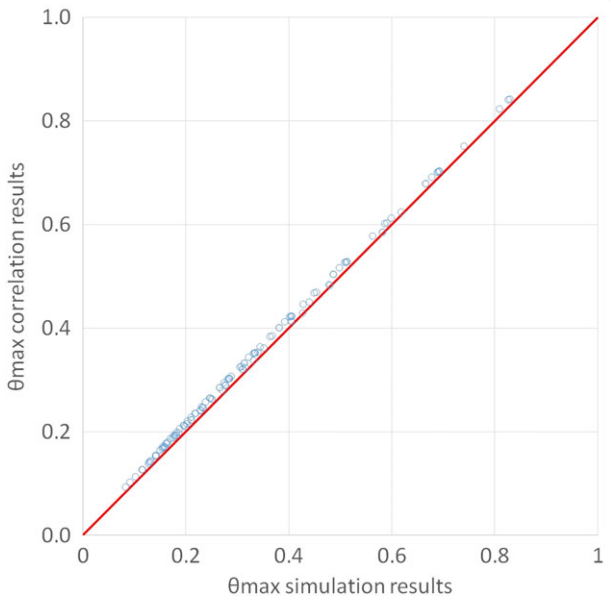

FIGURE 9 θ_{max} correlation results in comparison with simulation results [Colour figure can be viewed at wileyonlinelibrary.com]

The results in terms of the dimensional T_{max} can be easily obtained combining Equations 14 and 16:

$$T_{max}(D_{eq},Z) = T_{ext} + f_1(D_{eq})\cdot\left[1-\exp\left(g_1(D_{eq})Z^{h_1(D_{eq})}\right)\right]\cdot\Delta T. \quad (20)$$

3.3 | $\theta_{bottom}(r^*)$ results and proposed correlations $T_{bottom}(r)$ and Q_{bottom}

The results obtained with the numerical simulations for the evolution of the normalized ND temperature θ/θ_{max} in ND radial direction $r^* = r/R$ are analyzed in this section. Using this normalized ND temperature, all bottom temperature profiles pass through the points ($r^* = 0$, $\theta/\theta_{max} = 1$) and ($r^* = 1$, $\theta/\theta_{max}\rightarrow 0$). A correlation as a function of the ND independent variables D_{eq} and Z is proposed to estimate the simulated results.

In Figure 10, the simulation results in dimensionless terms are shown for the evolution of the normalized ND temperature with r^* for four different values of D_{eq}, where Z is fixed. Results show a decrease in the values of θ/θ_{max} in all the range of r^* for increasing values of D_{eq}. It is observed that the reduction in θ/θ_{max} is higher for lower values of D_{eq} and also that for values of D_{eq} equal or higher than 0.67 the temperature profiles are approximately the same. This observation is coherent with the fact that although heat loss decreases as the insulation thickness increases, the heat loss decreases more rapidly with smaller insulation thicknesses values (in ND terms, $D_{eq} = 0.17$ and $D_{eq} = 0.33$) in comparison with higher insulation thicknesses (in ND terms, $D_{eq} = 0.67$ and $D_{eq} = 1.17$).

In Figure 11, the simulation results in dimensionless terms are shown for the evolution of the ND temperature with r^* as a function of four different values of Z, where

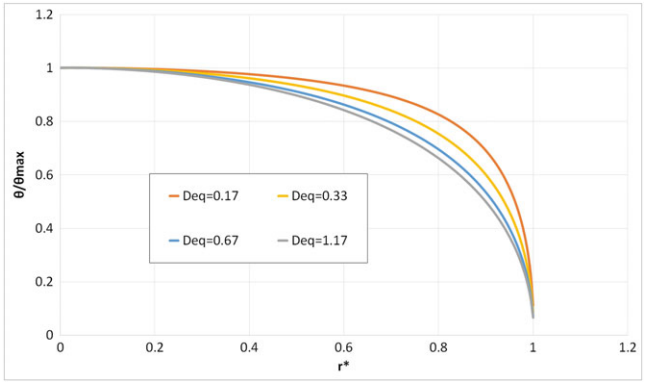

FIGURE 10 Evolution of θ/θ_{max} with r^* for different D_{eq} values, Z fixed [Colour figure can be viewed at wileyonlinelibrary.com]

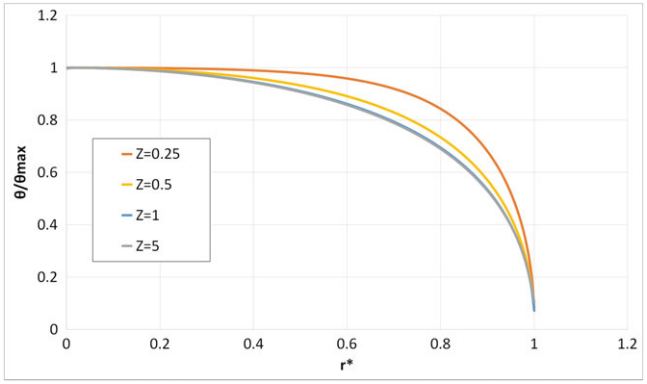

FIGURE 11 Evolution of θ/θ_{max} with r^* for different Z values, D_{eq} fixed [Colour figure can be viewed at wileyonlinelibrary.com]

D_{eq} is fixed. Results show a decrease in the values of θ/θ_{max} in all the range of r^* for increasing values of Z. It is observed that the reduction in θ/θ_{max} is higher for lower values of Z and also that for values of Z equal or higher than 1 the temperature profiles are approximately the same, in concordance with the behavior observed for θ_{max} previously in Figure 8.

In a preliminary analysis, different mathematical functions were tested against the simulation results shown in Figure 11 for a fixed value of Z. From this preliminary analysis, a mathematical function of the form presented in Equation 21 is selected to properly fit the simulation results (c_4 is constant for each fixed D_{eq} and Z values).

$$\theta_{bottom}(r^*) = \theta_{max}\left(1-r^{*2}\right)^{(c_4)} \tag{21}$$

The proposed correlation for $\theta_{bottom}(r^*)$ has the form

$$\theta_{bottom}(r^*) = \theta_{max}\left(1-r^{*2}\right)^{f_2(D_{eq},Z)} \tag{22}$$

where θ_{max} can be obtained with the functions defined in section 3.2.2 and $f_2(D_{eq},Z)$ is a function of the ND insulation level and the ND depth to water table defined in Equation 23:

$$f_2(D_{eq},Z) = \frac{0.47\cdot D_{eq}}{0.25+D_{eq}}\cdot\left[1-\exp\left(-4.55\cdot Z^{1.27}\right)\right]. \tag{23}$$

Equivalently, Equation 22 can be expressed in dimensional form, by substituting Equation 13 and $r^* = r/R$ and clearing $T_{bottom}(r)$:

$$T_{bottom}(r) = T_{stg} + \left[\theta_{max}(D_{eq},Z)\cdot\left(1-\frac{r^2}{R^2}\right)^{f_2(D_{eq},Z)} - 1\right]\cdot\Delta T \tag{24}$$

where θ_{max} and function f_2 only depend on the ND parameters D_{eq} and Z.

Total bottom heat losses are inferred by substituting the expression of Equation 24 in the integral of Equation 12 and solving it:

$$\begin{aligned} Q_{bottom} &= \int_{r=0}^{r=R}\frac{\left(T_{stg}-T_{bottom}(r)\right)}{R_{ins}}2\pi r\,dr \\ &= \pi R^2\frac{\Delta T}{R_{ins}}\left(1-\frac{\theta_{max}}{f_2(D_{eq},Z)+1}\right) \\ &= \pi R^2\frac{\Delta T}{R_{ins}}\cdot f_3(D_{eq},Z) \end{aligned} \tag{25}$$

where the term in brackets can be interpreted as a dimensionless reduction factor $f_3(D_{eq},Z)$ of the total heat bottom losses assuming an effective temperature difference $\Delta T = T_{stg} - T_{ext}$.

$$f_3(D_{eq},Z) = 1-\frac{\theta_{max}}{f_2(D_{eq},Z)+1}. \tag{26}$$

Alternatively, from Equation 25, it is derived in Equation 26 the expression for the total bottom heat losses per unit area:

$$\begin{aligned} q_{bottom} &= \frac{\Delta T}{R_{ins}}\left(1-\frac{\theta_{max}}{f_2(D_{eq},Z)+1}\right) \\ &= \frac{\Delta T}{R_{ins}}f_3(D_{eq},Z). \end{aligned} \tag{27}$$

A slight modification of Equations 25 and 27 is proposed for the correlation of Q_{bottom} and q_{bottom} in order to adjust the results in a way that the results are conservative in comparison to the simulation results. In Equations 28 and 29, the final expressions for the Q_{bottom} and q_{bottom} correlations as a function of the ND variables D_{eq} and Z are shown:

$$Q_{bottom} = 1.01\cdot\pi\cdot R^2\frac{\Delta T}{R_{ins}}f_3(D_{eq},Z) \tag{28}$$

$$q_{bottom} = 1.01\cdot\frac{\Delta T}{R_{ins}}f_3(D_{eq},Z) \tag{29}$$

Q_{bottom} correlation results are compared with the simulation results in Figure 12, where the 45° red solid line indicates a perfect fit between them.

Coefficients used in the proposed correlation have been adjusted in a way that the results are conservative, obtaining values of Q_{bottom} higher than the simulation results. A good agreement between the correlation and the simulation results was found with an average error of 0.7% and a maximum error of 2.9% in the worst case. Same deviations are obtained for results of q_{bottom}. For the pilot-scale tank described in subsection 2.3.2.4, correlation results (q_{bottom} = 63.36 W/m^2) agree with the

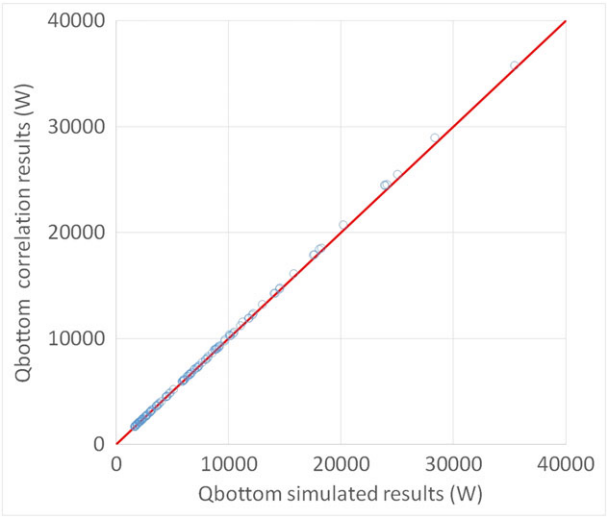

FIGURE 12 Q_{bottom} (W) correlation results in comparison with simulation results [Colour figure can be viewed at wileyonlinelibrary.com]

experimental results obtained by Prieto et al[19] ($q_{bottom} = 61.00\ W/m^2$) with an error of 3.9%.

3.4 | Summary and foundation design problem formulation

In this section, the proposed correlations are compacted and summarized as a function of the input parameters T_{ext}, D_{eq}, Z, ΔT, R, and R_{ins}, where the insulation and water table depth dimensionless variables are defined as: $D_{eq} = (t_{ins} \cdot \lambda)/(\lambda_{ins} \cdot R)$ and $Z = D'_{wt}/R$.

From Equations 17 to 20, the resulting correlation for the maximum temperature T_{max} is

$$T_{max} = T_{ext} + \frac{1.05}{1 + 1.49 \cdot D_{eq}} \cdot \left[1 - \exp\left(\left(-2.35 + \frac{0.6}{D_{eq}^{0.5}}\right) \cdot Z^{\frac{1.13 \cdot D_{eq}}{0.075 + 0.075 \cdot D_{eq}}}\right)\right] \cdot \Delta T. \tag{30}$$

From Equations 16 to 19 and 23 to 24, the resulting correlation for the bottom temperature as a function of the radial coordinate $T_b(r)$ is

$$T_b(r) = T_{stg} + \left\{\left\{\frac{1.05}{1 + 1.49 \cdot D_{eq}}\left[1 - \exp\left(\left(-2.35 + \frac{0.6}{D_{eq}^{0.5}}\right) \cdot Z^{\left(\frac{1.13 \cdot D_{eq}}{0.075 + 0.075 \cdot D_{eq}}\right)}\right)\right]\right\}\left(1 - \frac{r^2}{R^2}\right)^{\frac{0.47 \cdot D_{eq}}{0.25 + D_{eq}}} \cdot \left[1 - \exp\left(-4.55 \cdot Z^{1.27}\right)\right] - 1\right\} \Delta T \tag{31}$$

From Equations 16 to 19 and 23, 26, and 29, the resulting correlation for the bottom heat losses per unit area q_{bottom} is

$$q_{bottom} = 1.01 \cdot \frac{\Delta T}{R_{ins}} \left\{1 - \frac{\frac{1.05}{1 + 1.49 \cdot D_{eq}} \cdot \left[1 - \exp\left(\left(-2.35 + \frac{0.6}{D_{eq}^{0.5}}\right) \cdot Z^{\left(\frac{1.13 \cdot D_{eq}}{0.075 + 0.075 \cdot D_{eq}}\right)}\right)\right]}{\frac{0.47 \cdot D_{eq}}{0.25 + D_{eq}} \cdot [1 - \exp(-4.55 \cdot Z^{1.27})] + 1}\right\}. \tag{32}$$

The application of correlations presented in Equations 30 to 32 provides relevant information related to the thermal foundation tank design and can be used for different purposes. The direct application of Equations 30 to 32 provide an estimation of the thermal behavior for a given foundation design with any combination of fixed input parameters. In other cases, the foundation design is constraint to additional thermal requirements related to the maximum admissible temperatures in the soil underneath the tank and to maximum admissible heat loss per area. In most practical situations as the location, the soil characteristics, the operating temperature, and the tank size are fixed, only the insulation thickness can be changed in the design. Under these circumstances, the design problem consists of obtaining the minimum insulation thickness that fulfills the foundation thermal requirements, formulated in Equations 33 and 34.

Minimize insulation thickness

$$T_{max} < T_{max,adm} \tag{33}$$

$$q_{bottom} < q_{bottom,adm.} \tag{34}$$

In the next section, the proposed correlations are used, and the results for different combinations in the input parameters are analyzed for TES tanks applications.

3.5 | Parametric analysis

In this section, a parametric analysis is performed, and the variation of q_{bottom} is examined for the relevant variables of the problem: insulation thermal resistance, type of soil, tank radius, storage temperature, and depth to water table. The maximum temperature achieved underneath the insulation layer of 70°C, 80°C, 90°C, 100°C, 150°C, and 200°C are also indicated in the analysis in all the figures.

3.5.1 | Effect of the insulation thermal resistance

As previously mentioned, in most practical situations, only the insulation thermal resistance can be changed in the design, as the other parameters are predetermined. Figure 13 depicts the variation of q_{bottom} as a function of the insulation thermal resistance (R'_{ins}) for four different values of storage temperature (T_{stg}) typical in TES tanks operation. Storage temperatures of 292°C, 386°C, and 565°C are typical operation temperature ranges in commercial parabolic trough and solar tower applications, while 750°C is selected for illustrative purposed only. The soil is assumed to be unsaturated with constant thermal conductivity of $\lambda = 2$ W/mK. The rest of parameters, tank radius R, and exterior temperature are assumed to be constant: $R = 20$ m and $T_{ext} = 10$°C. Results show a decrease in q_{bottom} as R'_{ins} increases, showing an asymptotic trend, with higher reduction for lower values of R'_{ins} and lower reduction for higher values of R'_{ins}. Higher storage temperatures obviously produce higher thermal losses for a constant value of R'_{ins}. One of the main findings, based in the results of Figure 13, is that to achieve maximum temperatures below a certain value, a higher thermal insulation value is required but q_{bottom} remains approximately constant, especially for temperatures below 100°C. This result is true for any storage temperature. For example, q_{bottom} is limited to approximately 14 W/m^2 for maximum temperatures of $T_{max} = 100$°C for any storage temperature value in the range $T_{stg} = 292$°C to 750°C.

3.5.2 | Effect of the type of soil

Figure 14 shows the variation of q_{bottom} as a function of the soil thermal conductivity (λ) for five different values of insulation thermal resistance (R'_{ins}). Typical thermal conductivity values for clayey, sandy, and rocky soils are highlighted in the figure ($\lambda = 1.5$, 2, and 3.5 W/mK, respectively). Soil is assumed to be unsaturated. The rest of parameters are assumed to be constant ($R = 20$ m,

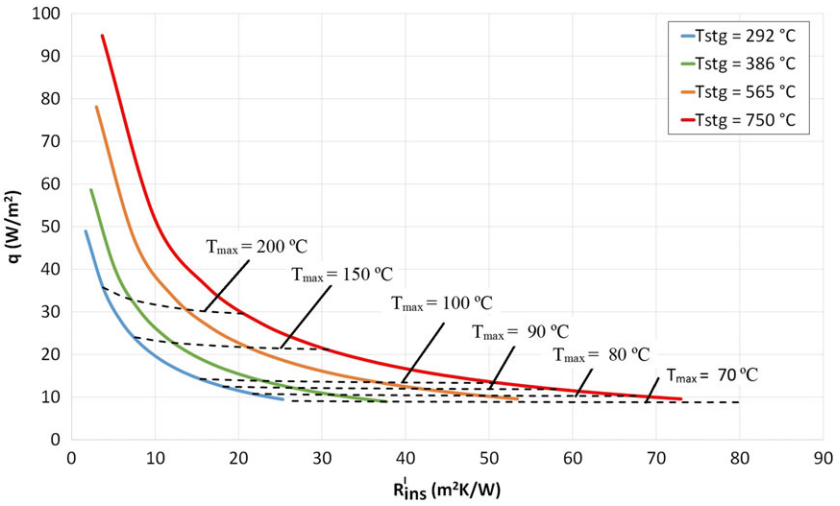

FIGURE 13 q_{bottom} (W/m^2) as a function of R'_{ins} for different T_{stg} ($\lambda = 2$ W/mk, $R = 20$ m, $T_{ext} = 10$°C) [Colour figure can be viewed at wileyonlinelibrary.com]

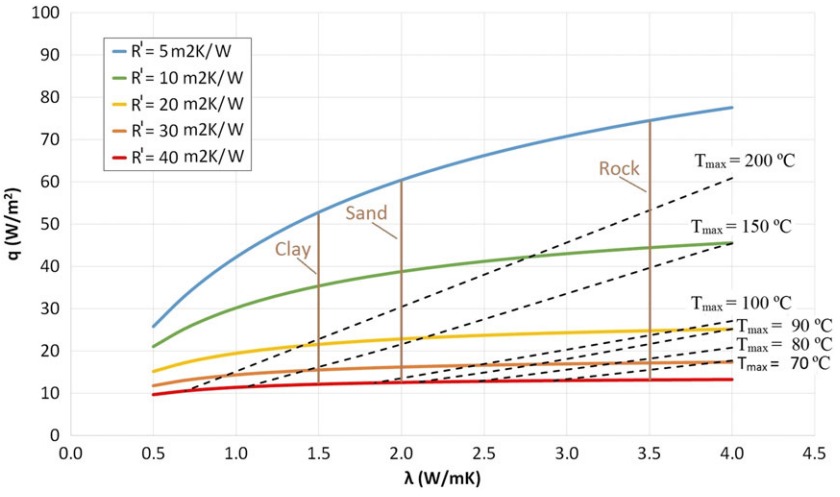

FIGURE 14 q_{bottom} (W/m^2) as a function of λ for different R'_{ins} ($T_{stg} = 565$°C, $R = 20$ m, $T_{ext} = 10$°C) [Colour figure can be viewed at wileyonlinelibrary.com]

T_{stg} = 565°C, and T_{ext} = 10°C). Higher soil thermal conductivities cause higher thermal losses, especially for lower insulation thermal resistances. For example, while for R'_{ins} = 5 m^2 K/W density heat losses vary from 54 W/m^2 to 75 W/m^2 for clayey and rocky soils, respectively, for higher insulations R'_{ins} = 40 m^2 K/W density heat losses remain approximately constant. Results show an approximately linear trend between the soil thermal conductivity and the density heat flux for a given value of the maximum temperature. For example, fixing the maximum temperature at T_{max} = 100°C, the rate q_{bottom}/λ is approximately constant and equal to 6.75.

3.5.3 | Effect of the tank size

Figure 15 shows the variation of q_{bottom} as a function of tank size characterized by the tank radius (R) for five different values of insulation thermal resistance (R'_{ins}). The rest of parameters are assumed to be constant: unsaturated soil of λ = 2 W/mK, T_{stg} = 565°C and T_{ext} = 10°C. Results show a decrease in q_{bottom} as R increases, with higher reduction for lower values of R'_{ins}. For example, while for R'_{ins} = 5 m^2 K/W density heat losses vary from 66 W/m^2 to 54 W/m^2 for tank radii of 15 to 25 m, for higher insulations R'_{ins} = 40 m^2 K/W density heat losses remain approximately constant, varying only from 13 to 12 W/m^2. For a given value of the maximum temperature, results show an asymptotic trend between the tank radius and the density heat flux. For example, fixing the maximum temperature at T_{max} = 100°C, while q_{bottom} varies from 27 to 17 W/m^2 for tank radii of 10 and 15 m (10 W/m^2 of difference), that difference in the case of tank radii of 15 and 20 m is only 5 W/m^2.

3.5.4 | Effect of the storage temperature

Figure 16 shows the variation of q_{bottom} as a function of the storage temperature (T_{stg}) for five different values of insulation thermal resistance (R'_{ins}). The rest of parameters are assumed to be constant: unsaturated soil of

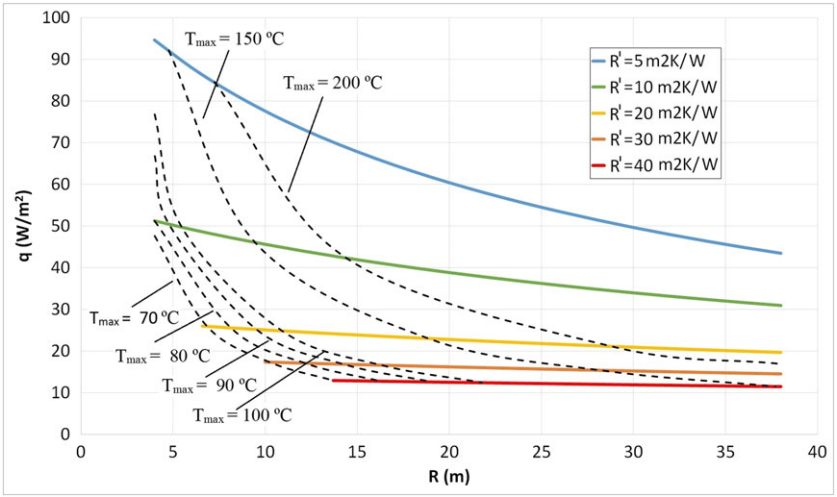

FIGURE 15 q_{bottom} (W/m^2) as a function of R for different R'_{ins} (λ = 2 W/mk, T_{stg} = 565°C, T_{ext} = 10°C) [Colour figure can be viewed at wileyonlinelibrary.com]

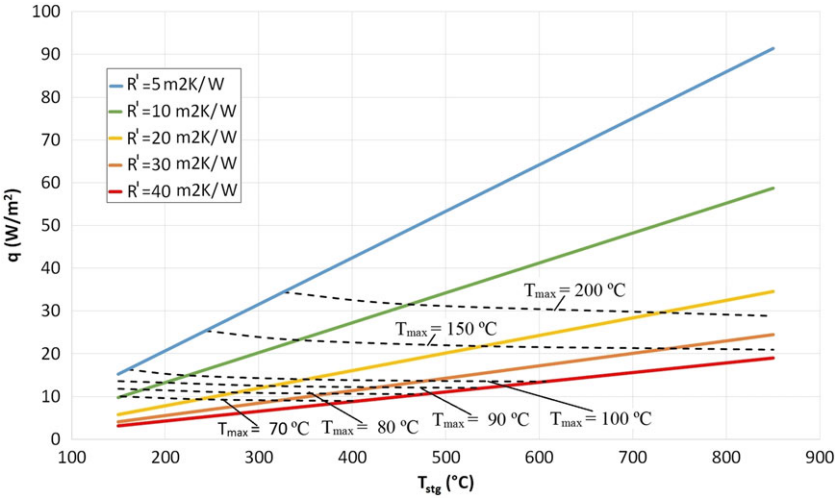

FIGURE 16 q_{bottom}(W/m^2) as a function of T_{stg} for different R'_{ins} (λ = 2 W/mk, R = 20 m, T_{ext} = 10°C) [Colour figure can be viewed at wileyonlinelibrary.com]

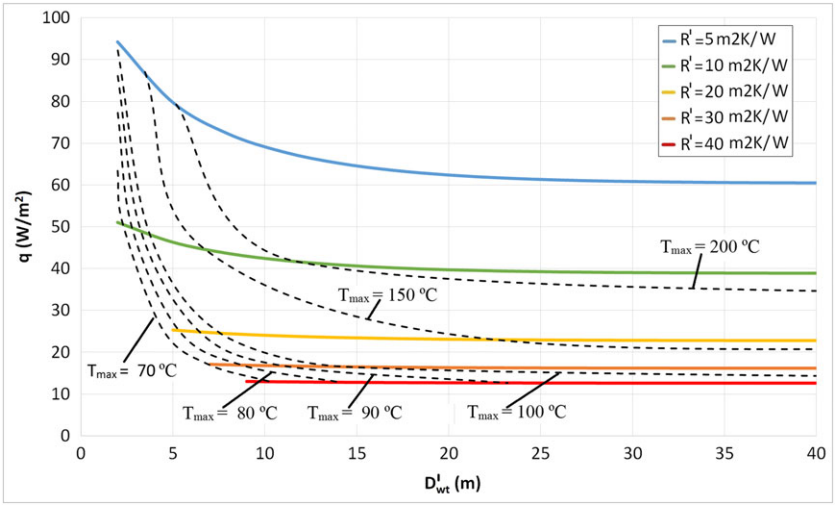

FIGURE 17 $q_{bottom}(W/m^2)$ as a function of D'_{wt} for different R'_{ins} ($\lambda = 2$ W/mk, $T_{stg} = 565°C$, $R = 20$ m, $T_{ext} = 10°C$) [Colour figure can be viewed at wileyonlinelibrary.com]

$\lambda = 2$ W/mK, $R = 20$ m and $T_{ext} = 10°C$. Results obviously show a linear increase in q_{bottom} as T_{stg} increases, as heat losses are proportional to the temperature difference. For a given value of the maximum temperature, results show an asymptotic trend between the tank radius and the density heat flux. For example, fixing the maximum temperature at $T_{max} = 100°C$, while q_{bottom} varies from 14.8 to 14.1 W/m^2 for storage temperatures of 300 and 400°C (0.7 W/m^2 of difference), the variation for storage temperatures of 400 and 500°C is only 0.4 W/m^2.

3.5.5 | Effect of the water table depth

Figure 17 shows the variation of q_{bottom} as a function of the water table depth (D'_{wt}) for five different values of insulation thermal resistance (R'_{ins}). The rest of parameters are assumed to be constant: $\lambda = 2$ W/mK, $R = 20$ m, $T_{stg} = 565°C$, and $T_{ext} = 10°C$. Results show a decrease in q_{bottom} as D'_{wt} increases. This decrease shows an asymptotic trend, especially significant for lower values of R'_{ins}, in the range of 5 to 20 m^{2}K/W. For higher values of R'_{ins} in the range of 20 to 40 m^{2}K/W the decrease of q_{bottom} with D'_{wt} is minimal and q_{bottom} is approximately constant. For a given value of the maximum temperature, results show an asymptotic trend between the water table depth and the density heat flux. For example, fixing the maximum temperature at $T_{max} = 100°C$, while q_{bottom} varies from 35 to 20 W/m^2 for water table depths of 5 and 10 m (15 W/m^2 of difference), the variation for water table depths of 10 and 15 m is only 6 W/m^2.

4 | CONCLUSIONS

This paper presents a new approach to predict the heat transfer of ground-coupled TES tank foundations. Mathematical correlations based on steady-state numerical solutions of the heat transfer beneath a TES tank have been proposed for the estimation of the tank foundation heat losses. The numerical model results were verified with other well-established benchmark problems with similar BCs[7,8] and validated with experimental data obtained from pilot plan scale TES tanks containing molten salts.[19] From the validation analysis, it was found an excellent agreement with the experimental results, with an error below 5.5%. Additionally, correlations for the radial evolution of the temperature underneath the insulation layer and for the maximum temperature achieved underneath the insulation layer are also presented separately. According to the authors' best knowledge, no publications can be found in the literature providing an analytical methodology that estimates these variables. Consequently, the proposed analytical correlations provide relevant information related to TES tank foundation design. Furthermore, the proposed correlations are function of well-defined and easy to calculate dimensionless parameters related to the tank insulation level (D_{eq}) and the dimensionless water table depth (D'_{wt}). The direct application of the proposed correlations provides important information related to the tank foundation design and can be used as a predesign tool to define an appropriate insulation level for given restrictions in the maximum allowable temperature and bottom heat losses, saving time, and cost on the engineering tank foundation design process. The effect of insulation thermal resistance, type of soil, tank size, storage temperature, and depth to water table on the maximum temperatures achieved underneath the insulation layer and the bottom heat losses per unit area was analyzed. In particular, it was found that the total bottom heat loss per unit area is decreased when the insulation level, the tank radius, or the water table depths are higher and are increased for higher soil thermal conductivities and storage temperatures.

Furthermore, it was found that to achieve the requirement of limiting the maximum temperature below a certain value, higher thermal insulation level is required for higher storage temperatures but q_{bottom} remains approximately constant, especially for maximum temperatures below 100°C.

ORCID

Christian Suárez http://orcid.org/0000-0003-1660-6296

REFERENCES

1. Acar C. A comprehensive evaluation of energy storage options for better sustainability. *Int J Energy Res*. 2018;1-15.
2. Dincer I. Thermal energy storage systems as a key technology in energy conservation. *Int J Energy Res*. 2002;26(7):567-588.
3. Suárez C, Iranzo A, Pino FJ, Guerra J. Transient analysis of the cooling process of molten salt thermal storage tanks due to standby heat loss. *Appl Energy*. 2015;142:56-65.
4. Kuravi S, Trahan J, Goswami DY, Rahman MM, Stefanakos EK. Thermal energy storage technologies and systems for concentrating solar power plants. *Prog Energy Combust Sci*. 2013;39(4):285-319.
5. Delsante AE, Stokes AN, Walsh PJ. Application of Fourier transforms to periodic heat flow into the ground under a building. *Int J Heat Mass Transf*. 1983;26(1):121-132.
6. Anderson BR. Calculation of the steady-state heat transfer through a slab-on-ground floor. *Build Environ*. 1991;26(4):405-415.
7. Hagentoft CE. Heat loss to the ground from a building. Doctoral dissertation. Lund University of technology: Sweden; 1988.
8. Chuangchid P, Krarti M. Steady-state component of three-dimensional slab-on-grade foundation heat transfer. *Trans Am Soc Mech Eng J Sol Energy Eng*. 2001;123(1):18-29.
9. ASHRAE. *ASHRAE Handbook of Fundamentals*. Atlanta, GA: ASHRAE; 1997.
10. CIBSE. *Guide A3: thermal properties of Buildings' structures*. London: CIBSE; 1986.
11. Powell KM, Edgar TF. Modeling and control of a solar thermal power plant with thermal energy storage. *Chem Eng Sci*. 2012;71:138-145.
12. Rovira A, Montes MJ, Valdes M, Martínez-Val JM, Varela F. On the improvement of annual performance of solar thermal power plants through exergy management. *Int J Energy Res*. 2014;38(5):658-673.
13. Demir M, Dincer I. Development and analysis of a new integrated solar energy system with thermal storage for fresh water and power production. *Int J Energy Res*. 2017;1-11.
14. Rosen MA, Dincer I. Exergy methods for assessing and comparing thermal storage systems. *Int J Energy Res*. 2003;27(4):415-430.
15. Schulte-Fischedick J, Tamme R, Herrmann U. CFD analysis of the cool down behaviour of molten salt thermal storage systems. In: ASME 2008 2nd International Conference on Energy Sustainability collocated with the heat transfer, fluids engineering, and 3rd energy nanotechnology conferences. American Society of Mechanical Engineers; 2008: 515–524.
16. Zaversky F, García-Barberena J, Sánchez M, Astrain D. Transient molten salt two-tank thermal storage modeling for CSP performance simulations. *Solar Energy*. 2013;93:294-311.
17. Rodríguez I, Pérez-Segarra CD, Lehmkuhl O, Oliva A. Modular object-oriented methodology for the resolution of molten salt storage tanks for CSP plants. *Appl Energy*. 2013;109:402-414.
18. Bonilla J, Rodríguez-García M-M, Roca L, de la Calle A, Valenzuela L. Design and experimental validation of a computational effective dynamic thermal energy storage tank model. *Energy*. 2017;152:840-857.
19. Prieto C, Miró L, Peiró G, Oró E, Gil A, Cabeza LF. Temperature distribution and heat losses in molten salts tanks for CSP plants. *Solar Energy*. 2016;135:518-526.
20. Suárez C, Pino FJ, Rosa F, Guerra J. Heat loss from thermal energy storage ventilated tank foundations. *Solar Energy*. 2015;122:783-794.
21. Herrmann U, Kelly B, Price H. Two-tank molten salt storage for parabolic trough solar power plants. *Energy*. 2004;29(5-6):883-893.
22. Kelly B, Kearney D. Thermal storage commercial plant design study for a 2-tank indirect molten salt system. Final Report, NREL; 2006.
23. Jacob R, Belusko M, Fernández AI, Cabeza LF, Saman W, Bruno F. Embodied energy and cost of high temperature thermal energy storage systems for use with concentrated solar power plants. *Appl Energy*. 2016;180:586-597.
24. Özişik MN. *Heat Conduction*. John Wiley & Sons; 1993.
25. Gabbrielli R, Zamparelli C. Optimal design of a molten salt thermal storage tank for parabolic trough solar power plants. *J Sol Energy Eng*. 2009;131(4):041001.
26. Pouloupatis PD, Florides G, Tassou S. Measurements of ground temperatures in Cyprus for ground thermal applications. *Renew Energy*. 2011;36(2):804-814.

How to cite this article: Suárez C, Pino J, Rosa F, Guerra J. Analytical approach to ground heat losses for high temperature thermal storage systems. *Int J Energy Res*. 2019;43:439–454. https://doi.org/10.1002/er.4278